

Chemical reaction and mixing inside a coalesced droplet after a head-on collision

Szu-I Yeh, Horn-Jiunn Sheen & Jing-Tang Yang

Microfluidics and Nanofluidics

ISSN 1613-4982

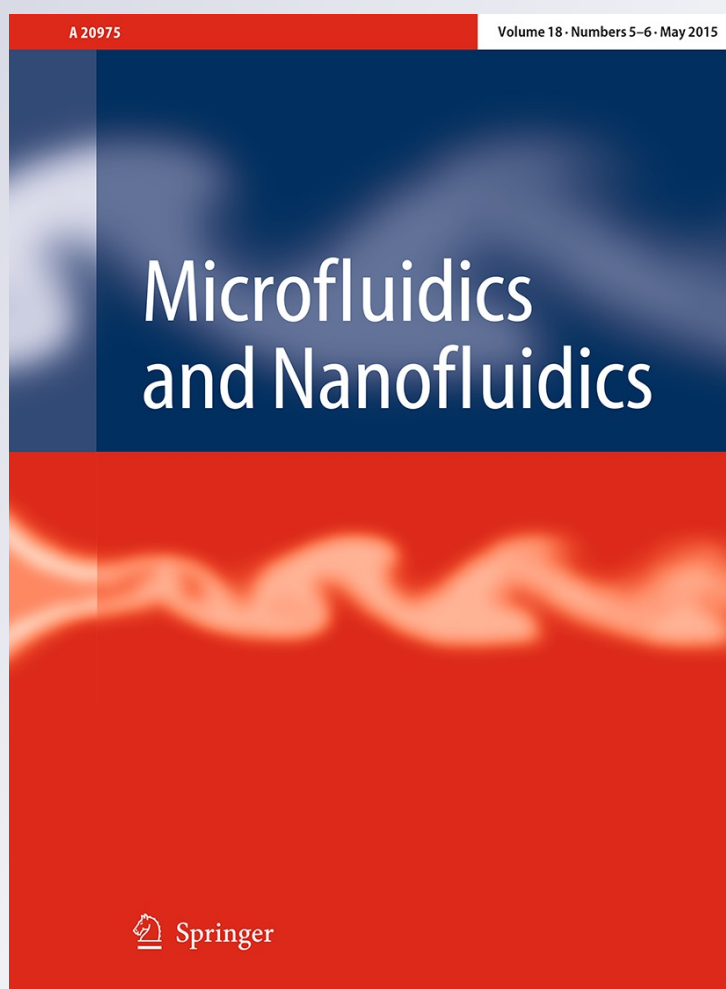
Volume 18

Combined 5-6

Microfluid Nanofluid (2015)

18:1355-1363

DOI 10.1007/s10404-014-1534-4



Your article is protected by copyright and all rights are held exclusively by Springer-Verlag Berlin Heidelberg. This e-offprint is for personal use only and shall not be self-archived in electronic repositories. If you wish to self-archive your article, please use the accepted manuscript version for posting on your own website. You may further deposit the accepted manuscript version in any repository, provided it is only made publicly available 12 months after official publication or later and provided acknowledgement is given to the original source of publication and a link is inserted to the published article on Springer's website. The link must be accompanied by the following text: "The final publication is available at link.springer.com".

Chemical reaction and mixing inside a coalesced droplet after a head-on collision

Szu-I Yeh · Horn-Jiunn Sheen · Jing-Tang Yang

Received: 15 September 2014 / Accepted: 7 December 2014 / Published online: 14 December 2014
© Springer-Verlag Berlin Heidelberg 2014

Abstract We investigated the phenomena of a chemical reaction inside a coalesced droplet after a direct (head-on) collision. A droplet containing an alkaline solution collided with a droplet containing a pH indicator on a surface with a wettability gradient. We used a high-speed camera to observe the color-changing reaction inside the coalesced droplet. Compared with a traditional dye-mixing test, the chemical reaction inside the coalesced droplet facilitated the mixing of two counter-reactive fluids and was more than 100 times as efficient as for unreactive fluids mixing inside the coalesced droplet. Instead of mere mixing, a chemical reaction inside a coalesced droplet is valuable for applications in a digital microfluidic open system. In droplet coalescence, the characteristics of the fluids and the ratio of volumes of two droplets caused a varied profile of the droplet coalescence, especially the neck curvature that affects the shape of the material interface between the two droplets at an initial phase. We observed the evolution of the chemical reaction with a varying radius of neck curvature inside the coalesced droplet. For the case of a small radius of neck curvature, the small interfacial area between two reactive fluids accumulated an intense heat of reaction and induced a rapid growth of the fingers. For the case of a large radius of neck curvature, the growth of fingers was slight and the interface was uniform across the large interfacial area. Our work illustrates a correlation between

the rate of chemical reaction and the profile of a coalesced droplet, which is a significant reference in droplet-based microfluidic systems for biochemical applications.

Keywords Droplets coalescence · Neck curvature · Chemical reaction front · Microfluidic mixing

1 Introduction

For their prospective applications in optics, electronics and *lab-on-a-chip*, microfluidic systems based on droplets have attracted much attention. Droplet microfluidic systems are expected to revolutionize procedures in a biological laboratory in allowing assays to become more rapid and free of error. Transport, collision and mixing of droplets are the key issues in the development of droplet-based microfluidic systems (Fair 2007; Fouillet et al. 2008; Huebner et al. 2008).

A collision between droplets is an important feature of various applications, such as spray combustion, polymer blending and manufacture of petrochemicals. The angle, velocity and distance between the colliding droplets cause droplet collision in three modes—coalescence, partial coalescence and bounce. Two dimensionless parameters—Weber number ($We = 2r\rho U_r^2/\sigma$, with droplet radius r relative velocity U_r , density ρ and surface tension σ of the liquid) and impact number ($B = X(r_1 + r_2)$, with distance X between the centers of mass of two droplets of radii r_1 and r_2 ; $B = 0$ signifies a direct collision)—are related to the modes of the droplet collision. Orme (1997) presented a map relating these three modes and the two parameters. Of these modes, droplet coalescence is the most important because of its applications in microfluidic systems for biochemical reactions in which mixing of reagents and

S.-I. Yeh · H.-J. Sheen (✉)
Institute of Applied Mechanics, National Taiwan University,
1 Sec. 4 Roosevelt Road, Taipei 106, Taiwan
e-mail: sheenh@ntu.edu.tw

S.-I. Yeh · J.-T. Yang (✉)
Department of Mechanical Engineering, National Taiwan
University, 1 Sec. 4 Roosevelt Road, Taipei 106, Taiwan
e-mail: jtyang@ntu.edu.tw

samples becomes the primary and definitive step. Sellier and Trelluyer (2009) hence used a simple scenario to describe the coalescence of sessile droplets and confirmed that the growth of the neck between the droplets conformed to a power law. Danov et al. (1993) applied a theoretical approach to the deformation of emulsion droplets before and after their coalescence; in their numerical calculations, they investigated the distance over which the droplet deformed and the total force acting between the droplets.

The mixing of biochemical reagents in a microfluidic device has been a critical step to improve the practicality of a micro-total-analysis system (μ TAS) or lab-on-a-chip. Researchers have tried to manipulate discrete droplets to achieve a rapid mixing of fluids through the internal motions of fluids caused by a rapid release of the interfacial force during the droplet coalescence or by a shear interaction with the surroundings (Hosokawa et al. 1999), but the merged droplet is typically not well mixed within a few seconds. EWOD-based (electrowetting-on-dielectric) devices have been developed to mix the merged droplet rapidly, accelerated through active manipulation of the droplets with linear electrodes and a varied aspect ratio of the droplets (Paik et al. 2003). Several researchers investigated the morphology and dynamics of the droplet collision and coalescence on a plane surface (Kapur and Gaskell 2007) or in a microchannel (Jose and Cubaud 2012) using plane-film (Tung et al. 2009), μ -PIV (Lu et al. 2008; Ortiz-Dueñas et al. 2010) and simulation tools (Monaco et al. 2014). We have already done much work on the measurement of coalescence, internal flows inside the coalesced droplet and evolution of three-dimensional mixing patterns inside a droplet (Lai et al. 2010a, b; Yeh et al. 2013; Huang et al. 2014). Because of the release of the heat of reaction and a product with a distinct density, a chemical reaction differs from a mixing behavior. The fingering instability driven by a chemical reaction inside the coalesced droplet is an interesting and unknown issue in a digital microfluidic system.

Among various methods to investigate rapid chemical reactions, rapid flow methods (Chance 1940) or relaxation methods (Eigen 1963) are commonly used for kinetic measurements. Recent applications of lasers enable a measurement of reactions on a femtosecond scale or less (Connelly et al. 1997). These methods are based on an assumption that a reaction occurs homogeneously in space, but some chemical reactions are known to develop spatial inhomogeneity (Zaikin and Zhabotinsky 1970; Ross et al. 1988). Neutralization of an acid with a base might drive hydrodynamic instabilities (Almarcha et al. 2010). These phenomena of inhomogeneity generally occur over a few seconds or even a few minutes. The evolution of a chemical reaction inside a droplet was investigated on letting a drop containing pH indicator bromothymol blue fall into an alkaline liquid; the results indicated that the observed deformation of

the droplet and the diffusion of heat play major roles during this early reaction stage (Tsuji and Muller 2012). Koh et al. (2013) investigated the platform that allows a ferrofluid droplet to be driven along a preprogrammed path; the chemical reaction (acid/base titration with a pH indicator) inside the droplet was demonstrated on this platform. Compared with mass transfer and mixing, the chemical reaction inside a droplet is important but less addressed of research.

In this work, we used a droplet collision to observe the short-term finger instability driven by a chemical reaction during droplet coalescence. One droplet containing an alkaline solution (NaOH, 0.1 M) collided with another droplet containing pH indicator phenolphthalein on a surface with a wettability gradient. The coalescence behavior, including varied neck curvature that affected the evolution of the chemical reaction, varied with the characteristics of the fluid (viscosity, surface tension, etc.) and the ratio of volumes of two droplets. For the case of a small radius of neck curvature, a finger formed with the thermal instability of the chemical front existing between two droplets and grew rapidly. For the case of a large radius of neck curvature, the finger also formed in a brief interval, but the growth of fingers was slow and uniform from the neck region. Our work illustrates that the finger instability driven by a chemical reaction is correlated with the material interface (neck curvature) between two fluids of the coalesced droplet. The experimental results shown in this work can serve as a reference basis for applications of droplet-based μ TAS or lab-on-a-chip systems.

2 Experiments

A sketch of the experimental apparatus appears in Fig. 1. A high-speed camera (Phantom v310) with an objective lens captured the views at a rate 3,200 fps and resolution

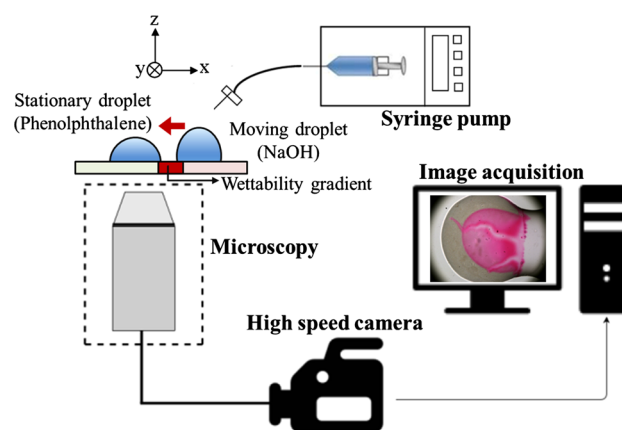
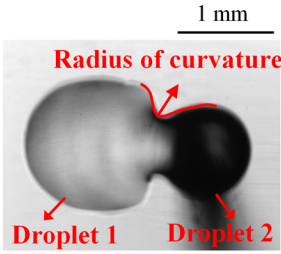


Fig. 1 Schematic diagram of the experiments. The chemical reaction caused color changes that we recorded with a high-speed camera

Fig. 2 Four experimental conditions tested for varied droplet size and curvature within the droplet coalescence. The neck curvature was measured at $t = 0.625$ ms after the droplets collided (see Fig. 3). The Weber number of the moving droplet (droplet 2) was 2.34×10^{-3}

	Droplet size 1 (μL)	Droplet size 2 (μL)	Radius of curvature, R (μm)
A	0.2	0.2	18.2 ± 1.4
B	0.3	0.2	34.5 ± 1.1
C	0.4	0.2	45.4 ± 1.7
D	0.5	0.2	48.8 ± 1.4

(a)



(b)

1600×1200 pixels ($1.6 \times 1.2 \text{ mm}^2$). The spatial resolution is $1.00 \mu\text{m}$ per pixel. The axial resolution of the system was approximately $5 \mu\text{m}$. Each experimental trial was performed 20 times; the reproducibility of the results is greater than 95 %.

Droplets were generated with a syringe pump (KDS220, KD Scientific) and microliter syringes (Hamilton 710RN). The platform for droplet control was fabricated with a modified vapor diffusion self-assembled monolayer (SAM) method. We fabricated a surface with a wettability gradient on a microscope slide (plain glass) so that light was transmitted from the bottom. This substrate also avoided optical distortion caused by the curved surface of a droplet that constitutes a major problem of quantitative visualization of a flow field within liquid droplets in an open system. The clean glass slide was placed vertically in a bottle containing decyltrichlorosilane (DTS) solution (0.025 % in dry toluene). The saturated SAM formed on the region immersed in the DTS solution. The other region above the liquid surface of the solution had a wettability gradient because DTS vapor diffused and deposited on the substrate. The contact angle of water on this surface varied from 105° to 55° within distance 0.4 mm. Further details of the fabrication of the gradient surface and of the measurement of the contact angle are reported elsewhere (Lai et al. 2010b; Yang et al. 2006).

One droplet, called a stationary droplet, was laid on the hydrophilic region of the surface; the other droplet (moving droplet) was subsequently dropped onto the hydrophobic region of the surface so that it moved spontaneously to collide with the stationary droplet, driven by the wettability gradient, from a hydrophobic to a hydrophilic region. The platform to control the point of droplet falling was a motorized xyz -positioning stage. The characteristics of fluid (viscosity, surface tension, etc.) and the ratio of volumes of two droplets caused varied profiles of the coalescing droplets. The evolution of the profile, in particular the varied neck curvature, modified the material interface between the two droplets during the droplet coalescence. The experimental conditions used in our work are shown in Fig. 2a. We varied the ratios of volumes of two droplets to control the material interface between two droplets during the droplet coalescence. The stationary droplet (droplet 1), of varied

volume, was collided with the moving droplet (droplet 2) of identical volume. The radius of curvature is defined in Fig. 2b that was captured at $t = 0.625$ ms after the droplets collided. The solution for droplet 1 was prepared from phenolphthalein (1 g; Sigma-Aldrich, Germany) dissolved in ethanol (100 mL). For droplet 1, its density is 833 kg/m^3 ; its surface tension is 29.52 mN/m ; and its viscosity is 1.24 cP at 25°C . For droplet 2, the solution contained sodium hydroxide (NaOH, 0.1 M; Showa Kako Corporation, Japan); its density is $1,021.5 \text{ kg/m}^3$; its surface tension is 46.35 mN/m ; and its viscosity is 1.15 cP at 25°C . As a control, we observed a droplet containing a yellow dye (Tartrazine) that collided with a droplet containing a blue dye (Indigo Carmine) on the same surface.

3 Results and discussion

During droplet coalescence, the evolution of the profile, especially the variation of the neck curvature, varied with the viscosity, surface tension and the ratio of volumes of the two droplets (Yeh et al. 2013). The sequential changes of the profile during droplet coalescence with experimental conditions A–D are shown in Fig. 3a–d, respectively. The triple-phase contact lines of the coalescing droplets were initially pinned and showed a neck region between the coalescing droplets. This region had a negative curvature along the interface, which induces a surface tension, thus leading the two droplets to coalesce to form a new and larger droplet. At 2 ms after the collision of the droplets, the neck region dispersed and the merged droplet slowly deformed to acquire a shape according to a minimum surface energy.

The radius of curvature of the neck region, measured at $t = 0.625$ ms after a collision, was related to the ratio of the volumes of the two droplets. Because of the balance of the surface tension, a larger difference of volume between two droplets caused a larger radius of curvature of the neck region (Fig. 3a–c). In our work, droplet 2 was automatically transported from a hydrophobic region to a hydrophilic region, restricted by the hydrophilic boundary. The boundary between the two regions was straight, which caused the shape of droplet 2 ($>0.3 \mu\text{L}$) not to be perfectly spherical

Fig. 3 Sequential images of coalescence behavior of two droplets of disparate size on the wettability gradient surface. Droplet 2 moves from *right* to *left*. **a–d** Represent experimental conditions A–D, respectively

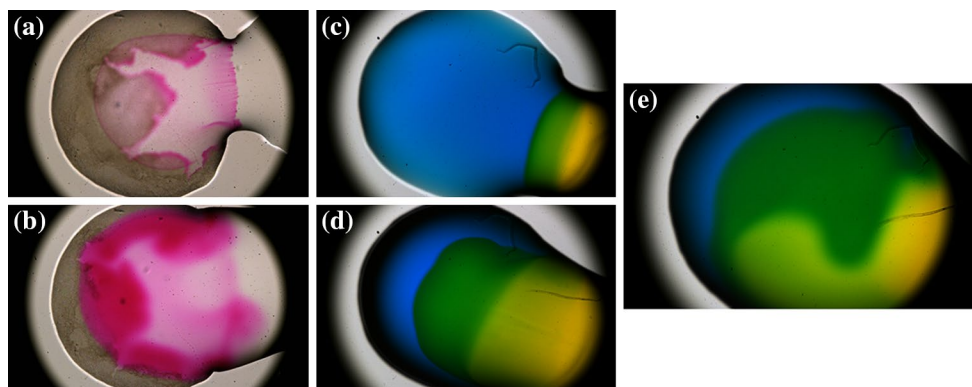
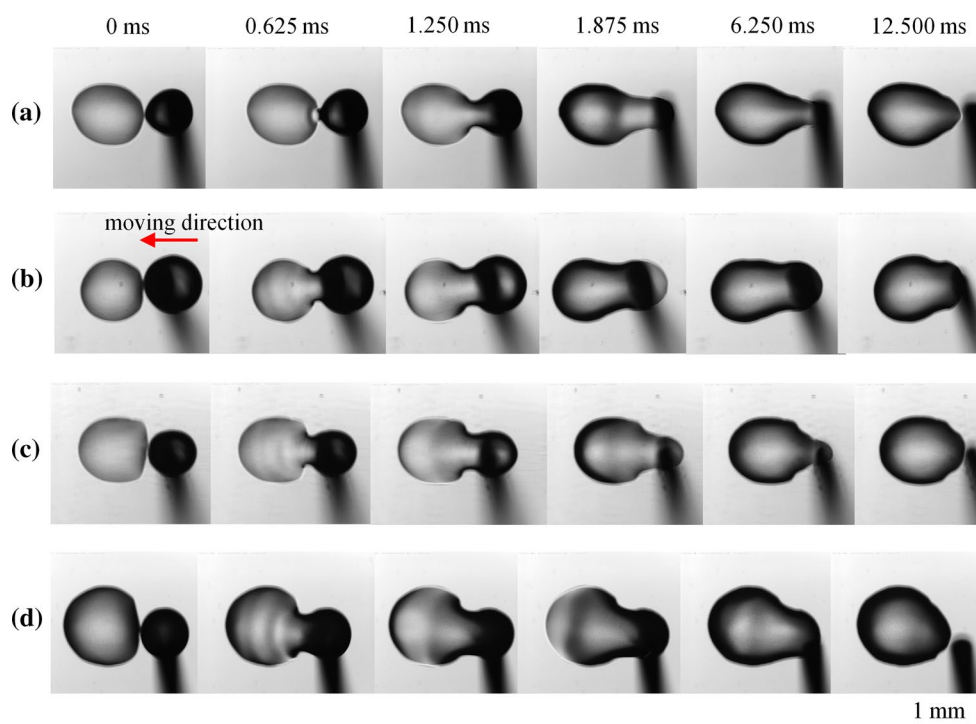


Fig. 4 Images of **a, b** a droplet (NaOH, 0.1 M, 0.2 μL) colliding with a phenolphthalein droplet (0.2 μL) at $t = 1.875$ ms, and 20.0 ms after the collision; **c–e** a *blue-dye* droplet (0.2 μL) that had collided

with a *yellow-dye* droplet (0.2 μL) at $t = 1.875$, 20.0 and 2,000.0 ms after the collision (color figure online)

and the trailing edge of droplet 2 to resemble a straight line along the boundary. Although we enlarged droplet 2, the coalescence profile of the droplet had only a small effect on the radius of curvature of the neck region (Fig. 3c, d).

Figure 4 shows images of the chemical reaction and the mixing of varied dyes inside the coalescing droplet. The blue-dye droplet collided with a yellow-dye droplet; the coalesced droplet is green when the two droplets were fully mixed. At $t = 1.875$ ms after a collision of the droplets, the chemical reaction induced fingers inside the coalescing droplet that are clearly visible (Fig. 4a). In contrast, the mixing of distinct dyes inside the coalesced droplet is dominated by a slow diffusion (Fig. 4c). When

the chemical reaction inside the coalesced droplet became saturated ($t = 20.0$ ms, Fig. 4b), the mixing inside the coalesced droplet was still slow (Fig. 4d). The patterns of color change due to the chemical reaction inside the droplet differed greatly from the mixing behavior inside the droplet. We used the normalized color-changed area (\bar{A}) to characterize the degree of chemical reaction and mixing (Fig. 5). In our previous work (Lai et al. 2010b; Yeh et al. 2013), we indicated that the mixing is driven sequentially by interior convection and diffusion; the convection endures less than 100 ms. In Fig. 5, the normalized color-changed area of distinct dyes has a linear growth in the convection-dominant period and slow exponential growth in the

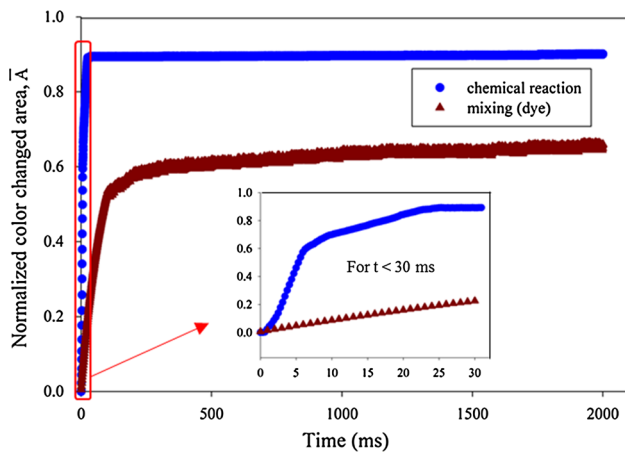


Fig. 5 Evolution of normalized *color-changed area* (\bar{A}) of chemical reaction and disperse dyes (color figure online)

diffusion-dominant period. The color-changed area induced by the chemical reaction at $t = 20$ ms is much larger than the fully mixed area at $t = 2,000$ ms, which means that the chemical reaction inside a coalesced droplet is more than 100 times as efficient as the mixing. The fingering instability driven by a chemical reaction inside the droplet is hence an important and notable phenomenon in droplet-based microfluidics.

Figures 6, 7, 8 and 9 show the initial behavior of the droplet and its color change due to chemical reaction in experimental conditions A–D. When droplet 2 (NaOH, 0.1 M) collided with droplet 1 (phenolphthalein), the color change was detected after 0.625 ms. The color change inside the coalesced droplet is apparently classifiable into two types: one is a spherical boundary along the leading edge of droplet 2 and the other involves the fingers from the

point of collision between the two droplets. Because of the inertial force of droplet 2 (the moving droplet), the color change along the leading edge of droplet 2 proceeded along the path of motion (right to left) of droplet 2 for all experimental conditions. The formation of fingers shows that a thermal instability of the chemical front existed between the two droplets for a brief period (<1 ms). The varied profile of the droplet coalescence affected the shape of the material interface between the two droplets and caused a varied distribution of thermal energy inside the coalescing droplet. For experimental condition A, the fingers spread and proceeded to the boundary of droplet 2. From the outset, the fingers were enveloped in the spherical boundary along the leading edge of droplet 2 (Fig. 6a–c). The heat of reaction accumulated inside the coalescing droplet, which caused the tips of the fingers to break through the envelope at 6.250 ms after a collision (Fig. 6d). Along with the termination of velocity caused by the inertial force of droplet 2, the evolution of the chemical reaction between the two solutions inside the coalesced droplet was dominated by diffusion, which led to a slow variation of color inside the coalesced droplet (Fig. 6e, f).

For experimental condition B, the fingers formed at $t = 1.250$ ms after a collision between the droplets. The small fingers formed and developed in an equatorial band on the coalesced droplet (Fig. 7b), which differs from experimental condition A, but the thermal instability inside the droplet caused the fingers to grow rapidly and the tips of the fingers to break through the envelope at 6.25 ms after the collision (Fig. 7c, d), similarly to experimental condition A.

For experimental conditions C and D, which have similar radii of neck curvature, the fingers formed along the neck region of the coalescing droplet (Figs. 8a, 9a). The

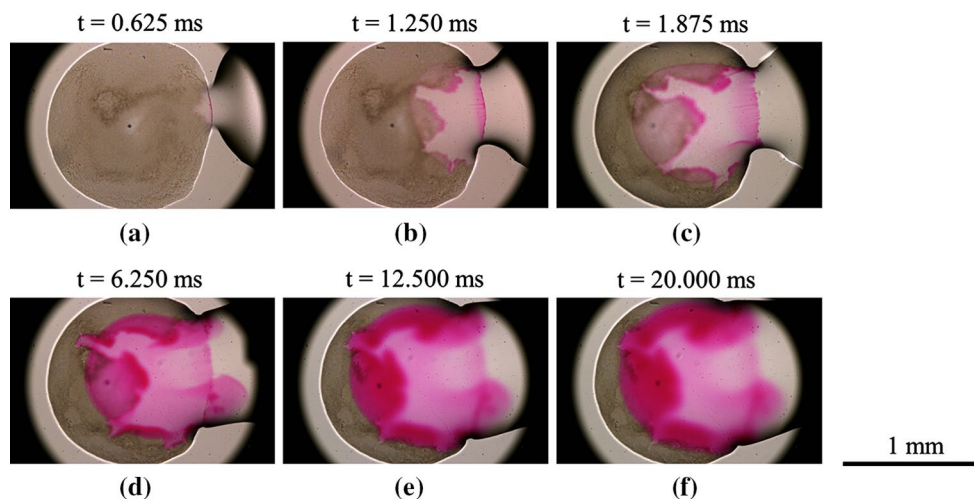


Fig. 6 Sequential images of experimental condition A; the droplet (NaOH, 0.1 M, 0.2 μ L) collided with the phenolphthalein droplet (0.2 μ L). Images a–f were captured at $t = 0.625$, 1.250, 1.875, 6.25, 12.5 and 20.0 ms after a collision

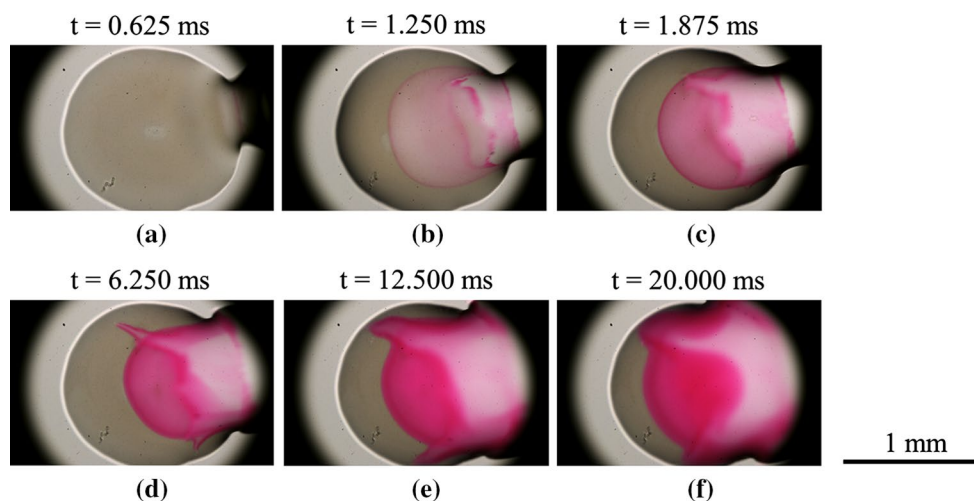


Fig. 7 Sequential images of configuration B; collision of the droplet (NaOH, 0.1 M, 0.2 μL) with the phenolphthalein droplet (0.3 μL). Images a–f were captured at $t = 0.625, 1.250, 1.875, 6.250, 12.50$ and 20.0 ms after a collision

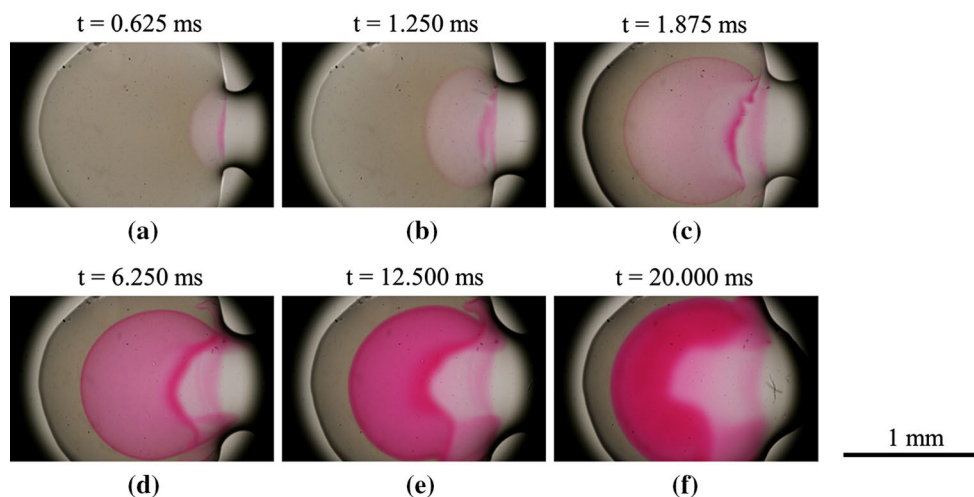


Fig. 8 Sequential images of experimental condition C; the droplet (NaOH, 0.1 M, 0.2 μL) collided with the phenolphthalein droplet (0.4 μL). Images a–f were captured at $t = 0.625, 1.250, 1.875, 6.250, 12.5$ and 20.0 ms after a collision

speed of finger propagation was less than the speed of the boundary of droplet 2 in both experimental conditions C and D (Figs. 8, 9). At $t = 6.250$ ms after a collision, the same as for experimental conditions A and B, the fingers grew rapidly and extended from either side of the neck region of the coalescing droplet (Figs. 8d, 9d).

Figure 10 shows enlarged images of the droplets at $t = 1.875$ ms after a collision in which the fingers are clearly visible after forming under varied experimental conditions. According to the radius of the neck curvature, the evolution of the finger instability is classifiable into two types: for the coalescing droplet of small radius of neck curvature, the small material interface between two solutions accelerated the accumulation of the heat of reaction and led to an extensive growth of the fingers (Fig. 10a, b)

and for the coalescing droplet of large radius of neck curvature, the large material interface between the two solutions led to a more gradual and uniform growth of the fingers (Fig. 10c, d).

We used a mixing length (L) and a reaction rate (Ra) to characterize the nonlinear dynamics of the finger-shaped front of the chemical reaction (De Wit 2004). The mixing length is defined as the distance between the tip and the rear of the fingers. The reaction rate is the normalized area of the reaction zone, defined as

$$Ra(t) = \frac{1}{DW} \int_0^D \int_0^W \bar{h} dx dy \quad (1)$$

in which $\bar{h} = 1$ if the concentration of a pixel exceeds a threshold, and zero otherwise; D and W are the sizes of the

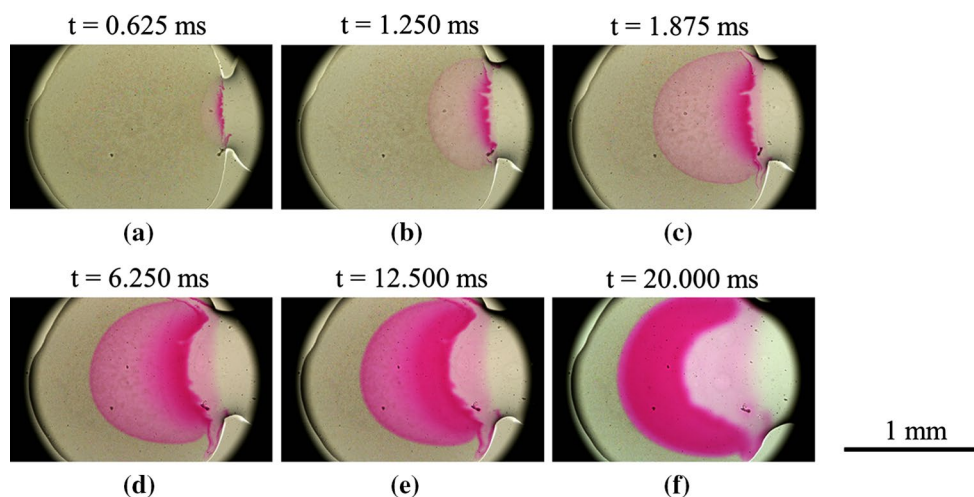


Fig. 9 Sequential images of experimental condition D; the droplet (NaOH, 0.1 M, 0.2 μL) collided with the phenolphthalein droplet (0.5 μL). Images a–f were captured at $t = 0.625, 1.250, 1.875, 6.250, 12.5$ and 20.0 ms after a collision

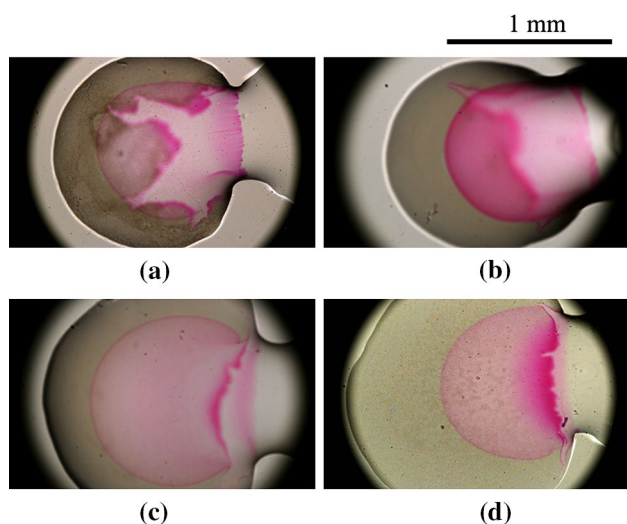


Fig. 10 Enlarged images a–d of experimental conditions A–D while the NaOH droplet (0.1 M) collided with the phenolphthalein droplet at $t = 1.875$ ms after a collision

droplet in directions x and y . The contact zone between the two solutions affected the rate of reaction. A reaction rate of value unity signifies that the fluids inside a coalesced droplet were fully reactive, whereas a rate zero signifies that fluids were entirely unreactive.

The development of a mixing length (L) for varied experimental conditions is shown in Fig. 11. Finger instability of two types caused two distinct evolutions of the mixing length. For the highly extended fingers of experimental conditions A and B, the fingering set is characterized by a linear growth of the mixing length with almost the same slope. The linear growth of fingers broke through the boundary between the two solutions at $t = 6.250$ ms

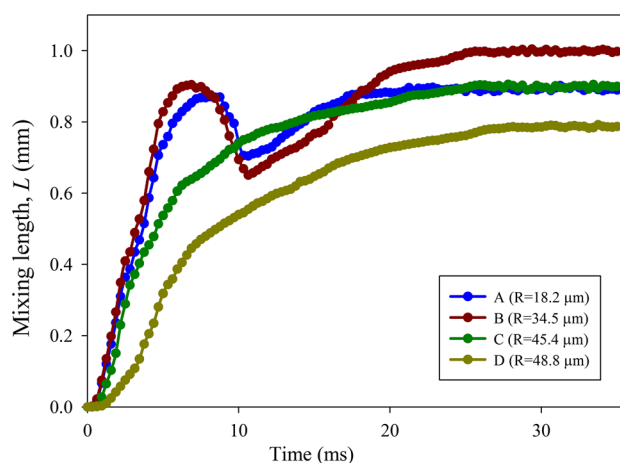


Fig. 11 Development of mixing length (L) for varied experimental conditions

after a collision. Because of the profile deformation of the coalescing droplet, the tails of the downward moving droplet suddenly decreased with a rapid movement of the rear of the droplet at $t = 6.875$ and 8.125 ms after a collision under experimental conditions A and B, respectively. The fingers ultimately grew slowly to the saturated mixing zone of a coalesced droplet. For the gradually grown fingers (experimental conditions C and D), the growths of the mixing length were fitted to an exponential decay, which initially decreased rapidly but tended to a steady condition about 10 ms after a collision. The growth of the mixing length in these experimental conditions coincided with a variation of the velocity field inside the coalescing droplet (Yeh et al. 2013).

The Damköhler number (Da) defines a ratio between the hydrodynamic and chemical time scales. The slope of the

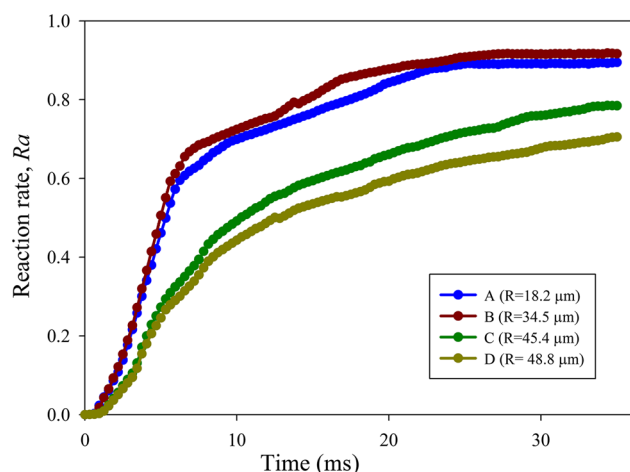


Fig. 12 Development of reaction rate (Ra) for varied experimental conditions

linear growth of the mixing length increased with larger Da , and the saturated mixing length decreased with a larger Da (Huebner et al. 2008). In our work, the droplet size and coalescence neck curvature did not vary with the Damköhler number; the slopes of the linear growth of mixing length were thus almost the same in experimental conditions A–D.

Figure 12 shows the reaction rate (Ra) as a function of time. The growth of the reaction rate was also fitted to an exponential formula, similar to the growth of the mixing length for experimental conditions C and D. For the highly extended fingers (experimental conditions A and B), the variations of reaction rate were similar. The rapid growth of fingers had an identical effect in accelerating the evolution of the chemical reaction, although the fingering patterns were not identical. For the gradually grown fingers under experimental conditions C and D, the reactions were slower than for experimental conditions A and B. The rates increased slowly and gradually for $t > 30$ ms, whereas the reaction rate inside the droplet was steady in experimental conditions A and B. The contact zone between the two solutions was increased in a fingered front that speeded the reaction and vice versa. The reaction rate and the mixing length interacted with each other: The chemical reaction generated the finger instability, and the fingering also had an influence on the reaction rate.

4 Conclusion

Patterned surfaces, fabricated with a SAM technique and having a wettability gradient, became a platform for the spontaneous transport and coalescence of droplets. A droplet containing an alkaline solution (NaOH, 0.1 M) moving

along the gradient surface struck another stationary droplet containing a pH indicator (phenolphthalein) on the hydrophilic region. We utilized a high-speed camera to investigate the growth of the chemical reaction fronts inside the coalescing droplets with varied coalescence profile. The neck curvature of the coalescence profile affects the shape of the material interface between the two droplets and the evolution of the chemical reaction. In this work, the chemical reaction rate inside the coalesced droplet proceeded more than 100 times as efficiently as the rate of fluid mixing inside the coalesced droplet.

The color change inside the coalescence droplet is classifiable into two types for all experimental conditions: a spherical boundary along the leading edge of moving droplet and a finger-shaped chemical reaction front from the point of collision of two droplets. The formation of fingers showed that a thermal instability of the chemical front existed between the two droplets for a brief period (< 1 ms). The varied profile of droplet coalescence affected the shape of the material interface between the two droplets and caused disparate thermal distributions and evolutions of finger patterns inside the coalescing droplet. According to the radius of the neck curvature, the evolution of the finger instability was also classifiable into two types: For the coalescing droplet with a neck curvature of small radius, the small material interface between the two solutions accelerated the accumulation of the heat of reaction and led to an extensive growth of the fingers and for the coalescing droplet with a neck curvature of large radius, the large interface of material between the two solutions led to a more gradual and more uniform growth of the fingers.

To characterize the nonlinear dynamics of the fingers, we used the mixing length (L) and the reaction rate (Ra). Finger instability of two types caused distinct evolutions of the mixing length. For the highly extended fingers under a small material interface between two counter-reactive fluids, the fingering set is characterized by a linear growth of the mixing length with almost the same slope. Because of the profile deformation of the coalescing droplet with a small radius of neck curvature, the tails of the downward moving droplet suddenly decreased with a rapid movement of the rear of the droplet. The fingers ultimately grew slowly to the saturated mixing zone of the coalesced droplet. For the fingers grown gradually with a large radius of neck curvature (large material interface between two droplets), the reaction rate initially decreased rapidly and tended to a steady condition about 10 ms after the collision of the droplets. The rate of reaction and the mixing length interacted with each other: The chemical reaction generated the finger instability, and the fingering also had an influence on the rate of reaction. In sum, the finger-shaped chemical reaction front inside the coalesced droplet evidently increased because of the rapid growth of fingers induced by

the accumulated intense heat of reaction with a small radius of neck curvature.

Instead of mass transfer and mixing, a chemical reaction inside a coalesced droplet is worthy of attention for a digital microfluidic open system. Our work illustrates a correlation between the growth and evolution of a chemical reaction and the profile (neck curvature) of a coalesced droplet, which is a significant reference in droplet-based microfluidic systems for biochemical use.

Acknowledgments National Science Council of Taiwan supported this work under Grant Number NSC-100-2120-M-002-013.

References

- Almarcha C, Trevelyan PM, Riolfo LA, Zalts A, El Hasi C, D'Onofrio A, De Wit A (2010) Active role of a color indicator in buoyancy-driven instabilities of chemical fronts. *J Phys Chem Lett* 1(4):752–757. doi:10.1021/jz900418d
- Chance B (1940) The accelerated flow method for rapid reactions. *J Frankl Inst* 229(6):737–766. doi:10.1016/S0016-0032(40)90963-2
- Connelly JP, Müller MG, Bassi R, Croce R, Holzwarth AR (1997) Femtosecond transient absorption study of carotenoid to chlorophyll energy transfer in the light-harvesting complex II of photosystem II. *Biochemistry* 36(2):281–287. doi:10.1021/bi962467l
- Danov KD, Petsev DN, Denkov ND, Ivanov IB, Borwankar R (1993) Coalescence dynamics of deformable brownian emulsion droplets. *Langmuir* 9(7):1731–1740. doi:10.1021/la00031a021
- De Wit A (2004) Miscible density fingering of chemical fronts in porous media: nonlinear simulations. *Phys Fluids* 16(1):163–175. doi:10.1063/1.1630576
- Eigen M (1963) Fast elementary steps in chemical reaction mechanisms. *Pure Appl Chem* 6(1):97–116. doi:10.1351/pac196306010097
- Fair RB (2007) Digital microfluidics: is a true lab-on-a-chip possible? *Microfluid Nanofluid* 3(3):245–281. doi:10.1007/s10404-007-0161-8
- Fouillet Y, Jary D, Chabrol C, Claustre P, Peponnet C (2008) Digital microfluidic design and optimization of classic and new fluidic functions for lab on a chip systems. *Microfluid Nanofluid* 4(3):159–165. doi:10.1007/s10404-007-0164-5
- Hosokawa K, Fujii T, Endo I (1999) Handling of picoliter liquid samples in a poly (dimethylsiloxane)-based microfluidic device. *Anal Chem* 71(20):4781–4785. doi:10.1021/ac990571d
- Huang CJ, Fang WF, Ko MS, Chou HYE, Yang JT (2014) A biocompatible open-surface droplet manipulation platform for detection of multi-nucleotide polymorphism. *Lab Chip* 14(12):2057–2062. doi:10.1039/c4lc00089g
- Huebner A, Sharma S, Srisa-Art M, Hollfelder F, Edel JB, deMello AJ (2008) Microdroplets: a sea of applications? *Lab Chip* 8(8):1244–1254. doi:10.1039/b806405a
- Jose BM, Cubaud T (2012) Droplet arrangement and coalescence in diverging/converging microchannels. *Microfluid Nanofluid* 12(5):687–696. doi:10.1007/s10404-011-0909-z
- Kapur N, Gaskell PH (2007) Morphology and dynamics of droplet coalescence on a surface. *Phys Rev E* 75(5):056315. doi:10.1103/PhysRevE.75.056315
- Koh WH, Lok KS, Nguyen NT (2013) A digital micro magnetofluidic platform for lab-on-a-chip applications. *J Fluid Eng* 135(2):021302. doi:10.1115/1.4023443
- Lai YH, Yang JT, Shieh DB (2010a) A microchip fabricated with a vapor-diffusion self-assembled-monolayer method to transport droplets across super-hydrophobic to hydrophilic surfaces. *Lab Chip* 10(4):499–504. doi:10.1039/B917624A
- Lai YH, Hsu MH, Yang JT (2010b) Enhanced mixing of droplets during coalescence on a surface with a wettability gradient. *Lab Chip* 10(22):3149–3156. doi:10.1039/C003729J
- Lu HW, Bottausci F, Fowler JD, Bertozzi AL, Meinhart C, Kim CJ (2008) A study of EWOD-driven droplets by PIV investigation. *Lab Chip* 8(3):456–461. doi:10.1039/B717141B
- Monaco E, Brenner G, Luo KH (2014) Numerical simulation of the collision of two microdroplets with a pseudopotential multiple-relaxation-time lattice Boltzmann model. *Microfluid Nanofluid* 16(1):329–346. doi:10.1007/s10404-013-1202-0
- Orme M (1997) Experiments on droplet collisions, bounce, coalescence and disruption. *Prog Energy Combust Sci* 23(1):65–79. doi:10.1016/S0360-1285(97)00005-1
- Ortiz-Dueñas C, Kim J, Longmire EK (2010) Investigation of liquid–liquid drop coalescence using tomographic PIV. *Exp Fluids* 49(1):111–129. doi:10.1007/s00348-009-0810-7
- Paik P, Pamula VK, Pollack MG, Fair RB (2003) Electrowetting-based droplet mixers for microfluidic systems. *Lab Chip* 3(1):28–33. doi:10.1039/B210825A
- Ross J, Müller SC, Vidal C (1988) Chemical waves. *Science* 240(4851):460–465. doi:10.1126/science.240.4851.460
- Sellier M, Trelluyer E (2009) Modeling the coalescence of sessile droplets. *Biomicrofluidics* 3(2):022412. doi:10.1063/1.3154552
- Tsuji K, Muller SC (2012) Chemical reaction evolving on a droplet. *J Phys Chem Lett* 3(8):977–980. doi:10.1021/jz300227q
- Tung KY, Li CC, Yang JT (2009) Mixing and hydrodynamic analysis of a droplet in a planar serpentine micromixer. *Microfluid Nanofluid* 7(4):545–557. doi:10.1007/s10404-009-0415-8
- Yang JT, Chen JC, Huang KJ, Yeh JA (2006) Droplet manipulation on a hydrophobic textured surface with roughened patterns. *J Microelectromech Syst* 15(3):697–707. doi:10.1109/JMEMS.2006.876791
- Yeh SI, Fang WF, Sheen HJ, Yang JT (2013) Droplet coalescence and mixing with identical and distinct surface tension on a wettability gradient surface. *Microfluid Nanofluid* 14(5):785–795. doi:10.1007/s10404-012-1096-2
- Zaikin AN, Zhabotinsky AM (1970) Concentration wave propagation in a two-dimensional liquid-phase self-oscillating system. *Nature* 225(5232):535–537. doi:10.1038/225535b0